American Society of Hematology
2021 L Street NW, Suite 900,
Washington, DC 20036
Phone: 202-776-0544 | Fax 202-776-0545
editorial@hematology.org

Conformation of von Willebrand factor in shear flow revealed with stroboscopic single-molecule imaging

Tracking no: BLD-2022-016969R1

Hans Bergal (Boston Children's Hospital, United States) Yan Jiang (Boston Children's Hospital, United States) Darren Yang (Wyss Institute, United States) Timothy Springer (Boston Children's Hospital, United States) Wesley Wong (Boston Children's Hospital and Harvard Medical School, United States)

Abstract:
von Willebrand factor (VWF) is a multimeric blood protein that acts as a mechanical probe, responding to changes in flow to initiate platelet plug formation. Previously, our labs had shown using single-molecule imaging that shear stress can extend surface-tethered VWF, but paradoxically we found that the required shear stress was higher than reported for free-in-flow VWF—an observation inconsistent with basic physical principles. To resolve this inconsistency critical to VWF's molecular mechanism, we measured free VWF extension in shear flow using PULSIS—**Pu**lsed **L**aser **S**troboscopic **I**maging of **S**ingle molecules. Here, laser pulses of different durations are used to capture multiple images of the same molecule within each frame, enabling accurate length measurements in the presence of motion blur. At high shear stresses, we observed a mean shift in VWF extension of less than 200 nm, much shorter than the multiple-micron extensions previously reported with no evidence for the predicted sharp globule-stretch conformational transition. Modeling VWF with a Brownian dynamics simulation, our results are consistent with VWF behaving as an uncollapsed polymer rather than the theorized compact ball. The muted response of free VWF to high shear rates implies that 1) the tension experienced by free VWF in physiological shear flow is lower than indicated by previous reports and 2) that tethering to platelets or the vessel wall is required to mechanically activate VWF adhesive function for primary hemostasis.

Conflict of interest: No COI declared

COI notes:

Preprint server: No;

Author contributions and disclosures: H.T.B., W.P.W., Y.J., and D.Y designed the research. H.T.B and Y.J. performed the experiments. H.T.B and D.Y ran simulations. W.P.W and H.T.B. drafted the manuscript. W.P.W., D.Y, Y.J, and H.T.B. analyzed data. H.T.B., Y.J., D.Y., T.A.S., and W.P.W. discussed the results and commented on the manuscript.

Non-author contributions and disclosures: No;

Agreement to Share Publication-Related Data and Data Sharing Statement: Email to the corresponding author

Clinical trial registration information (if any):

Conformation of von Willebrand factor in shear flow revealed with stroboscopic single-molecule imaging

Hans T. Bergal[1-3], Yan Jiang[2-4], Darren Yang[2,3,5], Timothy A. Springer[2-4], and Wesley P. Wong[2-5*]

Affiliations:
[1]Harvard Biophysics; [2]Program in Cellular and Molecular Medicine, Boston Children's Hospital; [3]Department of Biological Chemistry and Molecular Pharmacology, Blavatnik Institute at Harvard Medical School; [4]Department of Pediatrics, Harvard Medical School; [5]Wyss Institute for Biologically Inspired Engineering, Harvard University

*Correspondence: Wesley P. Wong, Center for Life Sciences, 3rd floor, Boston Children's Hospital, 3 Blackfan Circle, Boston, MA 02215; e-mail: wesley.wong@childrens.harvard.edu

Word counts for text: 3976

Word counts for abstract: 228

Figure count: 4

Reference count: 67

Key points:

- Free von Willebrand factor in flow extends gradually as shear stress increases, not abruptly with the presumed globule stretch transition.
- Polymer simulations suggest that VWF behaves as an uncollapsed, random chain with minimal monomer-monomer interactions.

Abstract:

von Willebrand factor (VWF) is a multimeric blood protein that acts as a mechanical probe, responding to changes in flow to initiate platelet plug formation. Previously, our labs had shown using single-molecule imaging that shear stress can extend surface-tethered VWF, but paradoxically we found that the required shear stress was higher than reported for free-in-flow VWF—an observation inconsistent with basic physical principles. To resolve this inconsistency critical to VWF's molecular mechanism, we measured free VWF extension in shear flow using PULSIS—**Pu**lsed **L**aser **S**troboscopic **I**maging of **S**ingle molecules. Here, laser pulses of different durations are used to capture multiple images of the same molecule within each frame, enabling accurate length measurements in the presence of motion blur. At high shear stresses, we observed a mean shift in VWF extension of less than 200 nm, much shorter than the multiple-micron extensions previously reported with no evidence for the predicted sharp globule-stretch conformational transition. Modeling VWF with a Brownian dynamics simulation, our results are consistent with VWF behaving as an uncollapsed polymer rather than the theorized compact ball. The muted response of free VWF to high shear rates implies that 1) the tension experienced by free VWF in physiological shear flow is lower than indicated by previous reports and 2) that tethering to platelets or the vessel wall is required to mechanically activate VWF adhesive function for primary hemostasis.

Introduction

von Willebrand factor (VWF) is a multimeric glycoprotein that circulates in blood and helps regulate hemostasis[1,2]. Consisting of 40-250 monomeric units arranged end-to-end, each VWF concatemer can have a contour length up to 15 μm[3–5]. Hydrodynamic forces regulate VWF's molecular mechanisms via tension-dependent binding. Binding partners include GPIbα for platelet recruitment[6–10], collagen for immobilization to damaged blood vessels[11,12], other VWF molecules for amplifying activation[13–15], and ADAMTS13 protease for VWF size-regulation[15–19]. VWF activation is premised upon its sensitivity to force, with conformational changes expected above a critical shear threshold. Extension is thought to expose binding sites, but sufficient tension is also required to allosterically activate binding to recruit platelets and initiate hemostasis.

Recently, Fu et al.[6] tethered VWF to a surface and measured VWF response to shear flow at the single-molecule level, monitoring extension and ability to bind the platelet-protein GP1bα. Surface-tethered VWF (figure 1A red) showed shear-dependent increases in extension up to the maximum shear stress applied (1280 dyn/cm^2). For reference, normal arterial shear stress is between 10-70 dyn/cm^2 but is estimated to reach higher than 400 dyn/cm^2 in injured arterioles[20].

In an earlier study[21], free VWF in pure shear flow was directly imaged. There appeared to be an extension of free VWF from a collapsed ball to an elongated filament ~15 μm in length, with abrupt extension at ~50 dyn/cm^2. Vascular injury was proposed to increase shear stress above this critical threshold, causing free-in-flow VWF to extend and adhere to the vessel wall at injury sites. A coarse-grained polymer model calibrated to match the extending behavior was used to model VWF[21,22]. The basic model of a collapsed polymer has been subsequently updated to simulate VWF behavior on a surface[23–25], in elongational flow[26–28], in shear flow[29–31] and size regulation through enzymatic cleavage[17,32,33].

These tethered and free VWF single-molecule experiments present a paradox: the putative shear stress required to extend free VWF was *lower* than the shear stress required to extend surface-tethered VWF (figure 1B). Simulations (figure 1C), based on Schneider et al's.[21] model were applied to both free and surface-tethered scenarios. They predict surface-tethered VWF should extend at shear stresses 100x lower than free VWF. Independent of simulations, basic physical arguments predict a lower shear stress to extend tethered vs. free polymers[30,34,35].

To resolve this discrepancy, we experimentally investigated the response of free VWF in shear flow using a new method to properly account for motion blur. Additionally, we updated the coarse-grained polymer model to match our new results and previously published single-molecule experiments. We find an uncollapsed polymer is sufficient to describe mesoscopic VWF behavior in flow, which complements a recent study that found evidence for a random coil description of VWF[36]. In contrast, models representing VWF as a collapsed polymer are difficult to reconcile with single-molecule data.

Our results indicate that single molecules of free VWF in physiological shear flow experience much lower internal tension than previous experiments and models predicted. This has major consequences for understanding the molecular mechanisms of hemostasis initiation, including the tension-dependent activation of VWF binding in flow and VWF size regulation, and further clinical significance for von Willebrand disease (VWD), thrombotic thrombocytopenic purpura (TTP), and Heyde's syndrome[4].

Methods

VWF and control preparation

Recombinant, therapeutic grade VWF was size-fractionated to select for longer multimers and labeled with Alexa 488 NHS-ester as described in Fu et al[6]. For the positive control, M13mp18RF DNA was labeled with YOYO-1. Fluorescent beads (diameter=0.11 µm determined by manufacturer) were used for the negative control. Imaging buffer was 60% (w/w) sucrose with 20 mM HEPES (pH 7.4), 150 mM NaCl, 0.02% Tween-20 and 0.5 mg/ml BSA.

Pulsed Laser Stroboscopic Imaging of Single molecules (PULSIS)

Molecules were imaged with a lab built TIRF microscope (60x oil immersion objective). A pressure-driven flow system was used to flow VWF through microfluidic channels (figure 2A). To correct for motion blur, we developed PULSIS (figure 2B-D), which images each molecule multiple times with different duration laser pulses. This enables us to build a relationship between the laser pulse duration and the observed streak length on a per molecule basis which is used to determine a “zero-pulse” or motion blur corrected length. Molecules were imaged with pulsed laser illumination, which followed a pattern of 1-on,3-off,1-on,3-off,2-on,3-off,3-on,3-off with the frequency of the pulse pattern tuned to the fluid velocity. (See supporting text section 1).

Image Analysis

PULSIS trajectories were analyzed with custom MATLAB scripts. Trajectories were manually selected, streak lengths were measured, and pulse duration (1,2,3) was assigned. A linear regression of pulse duration and measured lengths with fitting errors was performed, giving the particle velocity (slope) and the corrected molecule length (y-intercept).

Simulation

VWF multimers are represented by spherical beads, connected by a finitely extensible nonlinear elastic (FENE) potential with relevant hydrodynamic interactions[22]. Bead positions are updated according to a discretized Langevin equation based on the applied forces and random fluctuations from Brownian motion. The simulation uses a non-specific Lennard-Jones (LJ) potential, which accounts for a cohesive monomer-monomer attraction and excluded volume. (See supporting text S2).

Data Sharing

For data, contact wesley.wong@childrens.harvard.edu

Results

Pulsed Laser Stroboscopic Imaging of Single molecules (PULSIS)

To resolve the discrepancy between force scales of free and tethered VWF experiments, we developed a new single-molecule approach to investigate the length response of free VWF to shear flow. The primary experimental challenge is accurately measuring the lengths of molecules rapidly flowing through the field of view. The movement of molecules during image exposure causes motion blur, which is difficult to distinguish from molecule extension.

To correct motion blur at high shear rates we developed PULSIS, which images each molecule multiple times using a series of different duration laser pulses (figure 2A,B). The pulse pattern creates a series of fluorescent streaks that encode the length and velocity (dependent on distance from the vessel wall) of the molecule within a single frame. Based on the pulse duration and measured streak lengths, a linear regression gives the particle velocity (slope) and the length for a "zero-duration" pulse (y-intercept), i.e., the true length of the molecule. Example experimental PULSIS trajectories (figure 2C) show a fluorescently-labeled DNA molecule flowing across a single frame illuminated with the laser pulse pattern. The measured streak lengths at the corresponding pulse durations are fit to a line (streak length vs pulse duration), with the corrected extension given by the y-intercept (figure 2D). The corresponding linear fits of the image trajectories in figure 2C show linearized M13 DNA captured in two different orientations that differ in apparent length during tumbling in shear flow.

To test if PULSIS can distinguish between compact and elongated particles, we measured fluorescently labeled double-stranded DNA, in both the supercoiled and linearized states (figure 2E). Each molecule gives a motion-blur corrected length; these are aggregated together to build up a distribution of lengths (figure 2E). For example, the two trajectories (figure 2C-D) are single statistics from the distribution for linearized DNA in figure 2E. Supercoiled DNA remained compacted, giving a normal distribution with mean length L=0.26±0.25 μm. In contrast, linearized DNA had a broader distribution, with molecules up to ~1.7 μm and a shifted mean length L=0.58±0.38 μm, comparable to expected distributions for DNA in shear flow[37]. Broadening of the length distribution arises from the rotational component of shear flow, which causes polymers to tumble in cycles of extension and relaxation[38], with sampling of these states resulting in a broad distribution. To further validate PULSIS, fluorescent beads were imaged at shear stresses between 20-200 dyn/cm^2 (figure 2F). The average measurement at each shear stress was within 10 nm of the manufacturer's reported diameter of 110 nm and had no dependence on the applied shear stress.

Distinguishing collapsed vs. extended free-VWF can be difficult due to motion blur. One approach imaged fiduciary beads to subtract out motion-blur effects for VWF in shear flow[21]. However, small deviations in distance from the flow vessel wall between molecules and their fiducials (even less than the depth of field, supporting text S3) can result in large errors in perceived VWF length. In contrast, PULSIS uses each molecule as its own reference, without requiring comparison to other objects or precise knowledge of distance from the surface. Another approach used single short-illumination pulses to minimize the motion blur of VWF in flow[39]. However, this method has limited signal-to-noise ratio and retains some motion blur artifacts. By contrast, PULSIS can fully account for motion blur by extrapolation to infinitesimally short pulses while maintaining a strong signal-to-noise ratio. While others have used short, stroboscopic pulses to limit motion blur and track molecules[39–41], to our knowledge PULSIS is novel in using a pattern of different duration pulses to measure molecule lengths in flow.

Additionally, we used a 60% (w/w) sucrose solution to increase the viscosity of the imaging buffer by ~58 times compared to water[42] to study higher shear rates. This high-viscosity buffer applies equivalent shear stress at a 58-fold lower flow rate with correspondingly lower motion blur[6,39]. Surface-tethered VWF was imaged in both aqueous buffer and high-viscosity sucrose buffer at equivalent applied shear stresses (figure S2)[6]. Similar to previous studies[7], no differences in length were observed between molecules in the aqueous and sucrose buffer at the same shear stress, suggesting sucrose has minimal effects on the energetics of VWF extension. With the sucrose buffer and PULSIS, we can measure the lengths of free VWF molecules at shear stresses up to 200 dyn/cm^2, double the limit of previous experiments[39].

Measurement of VWF free in shear flow

Purified, fluorescently labeled VWF molecules were imaged with PULSIS at shear stresses of 20-200 dyn/cm^2(figure 3A), ranging from low arterial to pathological shear stresses[43]. Above 200 dyn/cm^2, the signal-to-noise ratio was too low for reliable data. However, this is still twice the highest shear stress imaged in previous studies of VWF free in flow[39]. The underlying size-distribution of VWF was estimated based on the length of tethered VWF molecules, with some molecules at least 6 µm in length (figure S2B).

At the lowest shear stress, the measured length distribution was Gaussian with mean and standard deviation L=0.15±0.17 µm. We interpret this distribution as containing compact VWF molecules, with the variance resulting primarily from measurement error. At 50 dyn/cm^2, the measured mean increased by 30 nm to 0.18 µm, dramatically less than the ~10 µm increase suggested[21] (figure 3B). At 200 dyn/cm^2, the highest shear stress measured, the mean length had shifted to 0.29 µm. Between 20 and 200 dyn/cm^2, the standard deviation increased from 0.16 to 0.41 µm, indicating the distributions were broadening. Like linearized DNA, the length distributions broaden at higher shear stresses as the VWF tumbles. The distributions are convolutions of the measurement error, the underlying VWF size distribution, and the tumbling of individual molecules.

The distributions at each shear stress were compared using the nonparametric Mann-Whitney U test for statistical significance. The test calculates the probability that the length distributions at two given shears are the same (figure 3D). Distributions at similar shear (80 dyn/cm^2 vs. 100 dyn/cm^2) are statistically similar (p=0.91). Large changes in shear stress, for example, 50 vs. 150 dyn/cm^2, give statistically different distributions (p<0.001), indicating the length distribution changes a marginal but statistically significant amount over the shear range explored.

We observed a small population of VWF molecules with a measured length of ∼2 µm (figure 3A, E-F), consistent with length heterogeneity in the VWF concatemers and suggesting some elongation in this subset at 100-200 dyn/cm^2. Comparing the 90th percentile of lengths between the 20 and 200 dyn/cm^2 shear stresses demonstrates a doubling in length (350 to 800 nm), while the median length changes by <100 nm (figure 3C).

Brownian Dynamics polymer simulations for VWF

Previous attempts to model VWF in flow have relied on coarse-grained Brownian Dynamics polymer simulations, as the massive size of VWF and the long timescales of physiological processes make full MD simulations unfeasible. The original free VWF in shear studies put forth a widely used Brownian dynamics model[22]. With more single-molecule experiments for VWF, we now have orthogonal experiments to test the model against[6,24,39].

The two parameters u (Lennard-Jones (LJ) interaction strength) and r (bead radius), make up a phase space which represents possible realizations of the simulation (figure 4A). Used to model basic intermolecular interactions[44], the Lennard-Jones potential is non-specific, meaning beads interact with all other beads. The LJ well-depth determines the strength of intermolecular interactions. With a large value (u> 0.314 k_BT), beads favorably interact to form a collapsed globule resistant to extension up to a critical shear stress, above which a sudden globule-stretch transition occurs[22,30,35]. VWF was proposed to behave like a collapsed polymer because a sharp transition was reported to occur in shear flow[21]. The simulation has been updated in more recent work to include features like A2 unfolding but continues to use collapsed polymers with LJ potentials between 0.52-1.44 k_BT [23–25,29,45].

At smaller interaction potentials ($u<0.314\ k_BT$), a polymer behaves as an uncollapsed polymer. At the Θ-point ($u=0.314\ k_BT$), the attractive and repulsive forces cancel out, and the polymer's dimensions match that of a simple ideal chain[46,47]. Unlike a collapsed polymer, an uncollapsed polymer's extension changes smoothly with increasing shear and does not have a sharp transition[38,48].

Shear resistance is also dependent on bead size. Larger beads experience more hydrodynamic drag than smaller beads causing elongation at lower shear stresses. In the original model, a large monomer attraction was used to get a sharp transition, which required a large bead of r=80 nm to fit the critical shear stress. Based on EM images from Fowler et al.[49] (figure 4B) and x-ray crystallography structures[1], a spherical radius of 80 nm overestimates two dimensions of VWF monomers. Recent models have attempted to correct this and reduced the bead radius to r=10-15 nm [23–25,29,45] but still overestimate the cross-section of VWF monomers (figure 4B).

We tested a polymer at the Θ-point ($u=0.314\ k_BT$) and optimized the bead size to best match the single-molecule experiments described below and found a radius of r=3.7 nm. This radius would require 8 spherical beads to make up a full monomer of 60 nm [49]. Notably, this bead size is similar to the size of the 11 domains in each VWF monomer, which range from 1.5-3 nm in radius[1,50]. We also evaluated the original Brownian dynamics model ($u=2.08\ k_BT$, r=80 nm) [21,22] and a revised-LJ model ($u=2.08\ k_BT$, r=14 nm) with a smaller radius representative of recent models[23–25,45]. The simulations are compared to three single-molecule experiments: previous measurements of surface-tethered VWF stretching in shear flow and subsequent relaxation[6] and measurements here of free VWF in shear flow. All simulations have a contour length of ~3 µm based on the average maximum extension length from surface extension experiments (figure S2B, expanded lengths in figures S3-4,S7,S9).

Polymer simulations for surface-tethered VWF in shear flow

Surface-tethered VWF in shear flow was simulated with the three models described above. Experimental data from Fu et al.[6] shows VWF extends little between 10-40 dyn/cm^2. Between 40-1280 dyn/cm^2, VWF requires an exponential increase in shear to achieve a linear length increase. Shear flow was applied to the tethered polymer models, then length in the flow direction was recorded and normalized by the length at the highest shear stress. When normalized by maximum extension, shear-extension curves of VWF are generally independent of length[6].

With a small bead size, our uncollapsed polymer experiences less hydrodynamic extensional force than other models and entropic effects are sufficient to resist extension without a cohesive potential. Like VWF, the simulated uncollapsed polymer's fractional extension scales logarithmically with shear stress and matches the data well (figure 4c). In contrast, due to large beads, the original LJ model unfolds completely by 10 dyn/cm^2 when tethered to the surface, at a shear stress ~100 times lower than experimentally observed. Furthermore, independent of bead radius, models with strong LJ interactions extend abruptly over a narrow range of shear stresses[22,35]. The revised-LJ model was optimized to reach the proper half-maximal extension at the same shear as VWF. This collapsed polymer extends ∼65% of its maximal length between 160 and 320 dyn/cm^2, showing an abrupt transition not experimentally observed.

Polymer simulations for free VWF in shear flow

The polymer simulations were further compared to our experimental measurements here of free VWF in shear flow. Shear flow was applied and the length distribution over time was recorded, as measured by the maximum length difference along the axis of flow. Since the contour length of the experimental VWF data is not known, the lengths are not normalized. The experimental data also represents a heterogenous distribution of sizes, making direct comparison difficult as polymer simulations have shown a size dependence for elongation in shear stress[30,51]. However, the qualitative behavior of each model is still informative.

Mean extensions of the simulated polymers in free shear were compared to the mean experimental length measurements (figure 4D). The original LJ model was specifically designed to exhibit large conformational changes in mean extension at shear stresses around 50-80 dyn/cm^2 and predicts a mean length change of 0.8 µm. The revised-LJ model, with parameters set to match the experimental surface stretching data, has a critical shear rate higher than the experiment and shows no change in mean length in the tested range. Our uncollapsed polymer model increases in mean extension by ~150 nm between 40-160 dyn/cm^2, qualitatively matching the observed behavior. Based on the uncollapsed polymer model, the mean tension under physiological shear stress was estimated to be <0.1 pN (supporting text S4, figure S5).

Polymer simulations for VWF relaxation

Polymer relaxation in the absence of flow provides orthogonal experimental VWF data to further test the predictions of models. Relaxation provides details on timescale and conformation. Experimental data was analyzed from Fu et al.[6] where VWF in a high-viscosity sucrose buffer is hydrodynamically stretched by a high shear stress and imaged as the molecule relaxes. Even in high viscosity buffer, VWF relaxes quickly in ~1 second. In our simulations (supporting text S5), we find the relaxation time scale is inversely correlated with the polymer bead size, consistent with a small bead radius to parameterize VWF (figure S6,S7). Furthermore, the relaxation conformation, based on the experimental fluorescence distribution of VWF, disagrees with the collapsed polymer simulation but is well-modeled by our uncollapsed polymer simulation (figure S8,S9).

Discussion

We developed PULSIS, an approach for measuring the lengths of molecules in high shear flow by measuring each molecule multiple times with different duration pulses. We then investigated VWF at shear stresses ranging from 20-200 dyn/cm^2, representing physiological to pathological shear stresses to capture relevant changes *in vivo*[20]. Qualitatively, the VWF length distribution shows no sharp globule-stretch transition near the previously reported 50 dyn/cm^2 threshold. Quantitatively, the change in mean length between 20-200 dyn/cm^2 is two orders of magnitude less than the previously reported values (0.17 vs 13 µm)[21]. This discrepancy may have resulted from motion blur artifacts in the previous work[21]. High shear rates coupled with limited axial resolution would make it difficult to account for motion blur with fiducial beads.

The small response of VWF to pure shear flow is a departure from the current perception within the field but still consistent with a majority of VWF literature. Length distributions, with a long tail with low micrometer lengths, is consistent with VWF free-in-flow experiments from Vergauwe et al.[39]. Furthermore, the measured mean extension of free VWF is less than the extension of tethered VWF reported by Fu et al.[6] at the same shear stress, resolving the force paradox discussed in figure 1B. A small response of VWF to shear stress is also consistent with small-angle neutron scattering experiments[52] which found no large-scale rearrangement at 30 dyn/cm^2 as well as dynamic light scattering experiments[7] which found no evidence for individual VWF extension at 60 dyn/cm^2.

Tension allosterically activates VWF binding to platelet proteins GPIb[6]. Furthermore, VWF cleavage by ADAMTS13 requires unfolding of the A2 domain for monomer cleavage, indicating that tension helps regulate VWF function[16]. Our results imply the tension experienced by free VWF in shear flow is lower than previously assumed; since tension depends on the difference in velocity between opposing ends of the molecule, a smaller extension should result in a comparably smaller tension[53].

Studies have observed VWF cleavage accelerated with shear stress[17,54]. However, other studies have observed no increase in ADAMTS13 cleavage with either high shear or elongational flow[55] but find that high turbulent flow results in VWF cleavage[56]. Based on our polymer model, the average tension at 80 dyn/cm^2, high arterial stress, is estimated to be <0.1 pN (figure S5), much lower than the force scale measured for A2 unfolding (f_b=1.1±0.2 pN)[16]. The estimated tension predicts that physiological shear does not dramatically bias on average the unfolded form of free-VWF A2 for VWF cleavage. However, it is unconfirmed whether physiological force could still play a role in accelerating the rate of cleavage or create a preference for cleavage of longer VWF molecules. The exact flow conditions and contributions from blood proteins like Factor VIII[60] needed for VWF cleavage require further experimental investigation.

VWF localizes to the area of vascular injury and recruits other clotting factors like platelets. VWF localization is likely driven by binding to collagen in the vessel wall that is exposed in injury[1]. Both flow-dependent[12] and flow-independent[61,62] VWF-collagen binding have been reported. Injury could expose collagen in the endothelium, allowing binding independent of flow. If the VWF-collagen binding rate has some tension dependence, shear stresses below 200 dyn/cm^2 are not predicted to have a significant role in accelerating binding. Supporting this, Colace and Diamond[12] observed minimal rates of VWF-collagen binding at a shear stress of 125 dyn/cm^2.

Extension and tension (~20 pN)[6] are necessary to shift the VWF A1 domain from a low affinity to a high affinity state for platelet protein GP1b binding[6]. Our results suggest single-molecules of free VWF alone do not exhibit shear-stress dependent binding to GP1b at physiological shear rates. Recruitment of platelets is likely only after VWF is attached to a surface, where the flow directly stretches VWF and higher tensions are reached. Interestingly, Nesbitt et al.[63] predominantly observed platelet aggregation on vessel walls at the point of stenosis, supporting the idea that both high flow and surface attachments are important for platelet aggregation.

We found no evidence for the sharp transition for free-in-flow VWF predicted by the LJ collapsed polymer simulations. Furthermore, based on the relaxation conformation and surface stretching behavior, the LJ collapsed polymer is not a suitable model for VWF. Meanwhile, our uncollapsed polymer model was consistent with previous VWF surface stretching-in-flow experiments[6], our own PULSIS data for free polymers in shear, and both time scale and conformation of relaxation from a stretched state. While the good agreement of single-molecule experiments with our uncollapsed polymer models do not constitute proof, an uncollapsed polymer is a sufficient description of the observed mesoscopic VWF dynamics in flow. Optimal bead size is on a similar scale as VWF domains, giving further agreement with physical observations of VWF. Our model suggests that VWF does not adopt a globular, collapsed form and monomers have minimal attractive interactions. This supports recent ultracentrifuge experiments where VWF behaved like a random coil[36] and is consistent with EM images of VWF[49].

The molecular mechanism of VWF activation is based on large conformational changes above a critical shear threshold to initiate hemostasis. However, we find no experimental evidence for a critical shear for large conformational changes in free-in-flow VWF—observed length changes are ~10 times smaller than previously thought. We find gradual length changes over a range of shear stress, consistent both in scale and shape with an uncollapsed polymer. Our results suggest free-flowing VWF molecules cannot act as a responsive sensor of shear stress for activation of hemostasis, invalidating a commonly held view of VWF activation. The field should investigate alternative initiation mechanisms, including the role of elongational flow near constriction sites, flow-independent binding to collagen in the vessel wall, and interaction with platelets.

Acknowledgements

We acknowledge the Harvard Medical School Orchestra 2 cluster for computing time. We thank data availability from Fu et al[6]. This work was supported by funding from NIH NIGMS R35 GM119537 (W. P. W), NIH HL148755 (T.A.S.) and NIH Molecular Biophysics Training Grant (NIH/NIGMS T32GM008313) (H.T.B).

Author contributions

H.T.B., W.P.W., Y.J., and D.Y designed the research. H.T.B and Y.J. performed the experiments. H.T.B and D.Y ran simulations. W.P.W and H.T.B. drafted the manuscript. W.P.W., D.Y, Y.J, and H.T.B. analyzed data. H.T.B., Y.J., D.Y., T.A.S., and W.P.W. discussed the results and commented on the manuscript.

Conflict-of-interest Disclosure

All the authors declare no competing financial interests.

ORCID profiles H.T.B., 0000-0002-5499-7833; Y.J., 0000-0002-2745-4323; D.Y., 0000-0002-2271-6910; T.A.S., 0000-0001-6627-2904; W.P.W., 0000-0001-7398-546X

References

1. Springer TA. von Willebrand factor, Jedi knight of the bloodstream. *Blood*. 2014;124(9):1412-1425. doi:10.1182/blood-2008-10-165621.

2. Yee A, Kretz CA. Von Willebrand factor: Form for function. *Semin Thromb Hemost*. 2014;40(1):17-27. doi:10.1055/s-0033-1363155

3. Sadler JE. Biochemistry and genetics of von Willebrand factor. *Annu Rev Biochem*. 1998;67:395-424. doi:10.1146/annurev.biochem.67.1.395

4. Sadler JE. New concepts in von Willebrand disease. *Annu Rev Med*. 2005;56:173-191. doi:10.1146/annurev.med.56.082103.104713

5. Reininger AJ. Function of von Willebrand factor in haemostasis and thrombosis. *Haemophilia*. 2008;14(SUPPL. 5):11-26. doi:10.1111/j.1365-2516.2008.01848.x

6. Fu H, Jiang Y, Yang D, Scheiflinger F, Wong WP, Springer TA. Flow-induced elongation of von Willebrand factor precedes tension-dependent activation. *Nat Commun*. 2017;8(1). doi:10.1038/s41467-017-00230-2

7. Shankaran H, Alexandridis P, Neelamegham S. Aspects of hydrodynamic shear regulating shear-induced platelet activation and self-association of von Willebrand factor in suspension. *Blood*. 2003;101(7):2637-2645. doi:10.1182/blood-2002-05-1550

8. Jiang Y, Fu H, Springer TA, Wong WP. Electrostatic steering enables flow-activated Von Willebrand factor to bind platelet glycoprotein, revealed by single-molecule stretching and imaging. *J Mol Biol*. 2019;431(7):1380-1396. doi:10.1016/j.jmb.2019.02.014

9. Dayananda KM, Singh I, Mondal N, Neelamegham S. von Willebrand factor self-association on platelet GpIbα under hydrodynamic shear: Effect on shear-induced platelet activation. *Blood*. 2010;116(19):3990-3998. doi:10.1182/blood-2010-02-269266

10. Interlandi G, Yakovenko O, Tu A, et al. Specific electrostatic interactions between charged amino acid residues regulate binding of von Willebrand factor to blood platelets. 2017;292:18608-18617. doi:10.1074/jbc.M117.797456

11. Fuchs B, Budde U, Schulz A, Kessler CM, Fisseau C, Kannicht C. Flow-based measurements of von Willebrand factor (VWF) function : Binding to collagen and platelet adhesion under physiological shear rate. *Thromb Res*. 2010;125(3):239-245. doi:10.1016/j.thromres.2009.08.020

12. Colace T V., Diamond SL. Direct observation of von Willebrand factor elongation and fiber formation on collagen during acute whole blood exposure to pathological flow. *Arterioscler Thromb Vasc Biol*. 2013;33(1):105-113. doi:10.1161/ATVBAHA.112.300522

13. Fu H, Jiang Y, Wong WP, Springer TA. Single-molecule imaging of von Willebrand factor reveals tension-dependent self-association. *Blood*. Published online 2021. doi:10.1182/blood.2021012595

14. Zhang C, Kelkar A, Neelamegham S. Von Willebrand factor self-association is regulated by the shear-dependent unfolding of the A2 domain. *Blood Adv*. 2019;3(7):957-968. doi:10.1182/bloodadvances.2018030122

15. Zheng Y, Chen J, Lopez JA. Flow-driven assembly of VWF fibre and webs in in vitro microvessels.

Published online 2015. doi:10.1038/ncomms8858

16. Zhang X, Halvorsen K, Zhang C-Z, Wong WP, Springer T. Mechanoenzymatic Cleavage of the Ultralarge Vascular Protein von Willebrand Factor. *Science (80-)*. 2009;324(June).

17. Lippok S, Radtke M, Obser T, et al. Shear-Induced Unfolding and Enzymatic Cleavage of Full-Length VWF Multimers. *Biophys J*. 2016;110(3):545-554. doi:10.1016/j.bpj.2015.12.023

18. Dong J fei, Moake JL, Nolasco L, et al. ADAMTS-13 rapidly cleaves newly secreted ultralarge von Willebrand factor multimers on the endothelial surface under flowing conditions. *Blood*. 2002;100(12):4033-4039. doi:10.1182/blood-2002-05-1401

19. Interlandi G, Ling M, Tu AY, Chung DW, Thomas WE. Structural Basis of Type 2A von Willebrand Disease Investigated by Molecular Dynamics Simulations and Experiments. 2012;7(10). doi:10.1371/journal.pone.0045207

20. Malek AM, Alper SL, Izumo S. Hemodynamic Shear Stress and Its Role in Atherosclerosis. *JAMA*. 1999;282(21):2035-2042.

21. Schneider SW, Nuschele S, Wixforth A, et al. Shear-induced unfolding triggers adhesion of von Willebrand factor fibers. *Proc Natl Acad Sci*. 2007;104(19):7899-7903. doi:10.1073/pnas.0608422104

22. Alexander-Katz A, Schneider MF, Schneider SW, Wixforth A, Netz RR. Shear-flow-induced unfolding of polymeric globules. *Phys Rev Lett*. 2006;97(13):1-4. doi:10.1103/PhysRevLett.97.138101

23. Morabito M, Dong C, Wei W, et al. Internal Tensile Force and A2 Domain Unfolding of von Willebrand Factor Multimers in Shear Flow. *Biophys J*. 2018;115(10):1860-1871. doi:10.1016/j.bpj.2018.09.001

24. Wang Y, Morabito M, Zhang XF, Webb E, Oztekin A, Cheng X. Shear-Induced Extensional Response Behaviors of Tethered von Willebrand Factor. *Biophys J*. 2019;116(11):2092-2102. doi:10.1016/j.bpj.2019.04.025

25. Dong C, Kania S, Morabito M, et al. A mechano-reactive coarse-grained model of the blood-clotting agent von Willebrand factor. *J Chem Phys*. 2019;151(12). doi:10.1063/1.5117154

26. Sing CE, Selvidge JG, Alexander-Katz A. Von Willlebrand adhesion to surfaces at high shear rates is controlled by long-lived bonds. *Biophys J*. 2013;105(6):1475-1481. doi:10.1016/j.bpj.2013.08.006

27. Kania S, Oztekin A, Cheng X, Zhang XF, Webb EB. Long time-scale study of von Willebrand factor multimers in extensional flow. *bioRxiv*. Published online 2020:2020.09.09.290304. https://doi.org/10.1101/2020.09.09.290304

28. Kania S, Oztekin A, Cheng X, Zhang XF, Webb E. Predicting pathological von Willebrand factor unraveling in elongational flow. *Biophys J*. 2021;120(10):1903-1915. doi:10.1016/j.bpj.2021.03.008

29. Ouyang W, Wei W, Cheng X, Zhang XF, Webb EB, Oztekin A. Flow-induced conformational change of von Willebrand Factor multimer: Results from a molecular mechanics informed model. *J Nonnewton Fluid Mech*. 2015;217:58-67. doi:10.1016/j.jnnfm.2015.01.009

30. Alexander-Katz A, Netz RR. Dynamics and instabilities of collapsed polymers in shear flow.

Macromolecules. 2008;41(9):3363-3374. doi:10.1021/ma702331d

31. Alexander-Katz A. Toward novel polymer-based materials inspired in blood clotting. *Macromolecules*. 2014;47(5):1503-1513. doi:10.1021/ma4007768

32. Huisman B, Hoore M, Gompper G, Fedosov DA. Modeling the cleavage of von Willebrand factor by ADAMTS13 protease in shear flow. *Med Eng Phys*. 2017;48:14-22. doi:10.1016/j.medengphy.2017.06.044

33. Radtke M, Lippok S, Rädler JO, Netz RR. Internal tension in a collapsed polymer under shear flow and the connection to enzymatic cleavage of von Willebrand factor. *Eur Phys J E*. 2016;39(3). doi:10.1140/epje/i2016-16032-7

34. Sing CE, Alexander-Katz A. Dynamics of collapsed polymers under the simultaneous influence of elongational and shear flows. *J Chem Phys*. 2011;135(1). doi:10.1063/1.3606392

35. Buguin A, Brochard-Wyart F. Unwinding of globular polymers under strong flows. *Macromolecules*. 1996;29(14):4937-4943. doi:10.1021/ma9600769

36. Parker ET, Lollar P. Conformation of the von Willebrand factor/factor VIII complex in quasi-static flow. *J Biol Chem*. 2021;296:100420. doi:10.1016/j.jbc.2021.100420

37. Schroeder CM, Teixeira RE, Shaqfeh ESG, Chu S. Dynamics of DNA in the Flow-Gradient Plane of Steady Shear Flow : Observations and Simulations. Published online 2005:1967-1978. doi:10.1021/ma0480796

38. Smith DE, Babcock HP, Chu S. Single-polymer dynamics in steady shear flow. *Science (80-)*. 1999;283(5408):1724-1727. doi:10.1126/science.283.5408.1724

39. Vergauwe RMA, Uji-i H, Ceunynck K De, Vermant J, Vanhoorelbeke K, Hofkens J. Shear-Stress-Induced Conformational Changes of von Willebrand Factor in a Water − Glycerol Mixture Observed with Single Molecule Microscopy. Published online 2014. doi:10.1021/jp5022664

40. English BP, Hauryliuk V, Sanamrad A, Tankov S, Dekker NH, Elf J. Single-molecule investigations of the stringent response machinery in living bacterial cells. *Proc Natl Acad Sci U S A*. 2011;108(31). doi:10.1073/pnas.1102255108

41. Xie XS, Choi PJ, Li GW, Nam KL, Lia G. Single-molecule approach to molecular biology in living bacterial cells. *Annu Rev Biophys*. 2008;37:417-444. doi:10.1146/annurev.biophys.37.092607.174640

42. Lee JC, Timasheff SN. The stabilization of proteins by sucrose. *J Biol Chem*. 1981;256(14):7193-7201. doi:10.1016/s0021-9258(19)68947-7

43. Sakariassen KS, Orning L, Turitto VT. The impact of blood shear rate on arterial thrombus formation. 2015;1.

44. Lennard-Jones JE. Cohesion. *Proc Phys Soc*. 1931;43(5):461-482. doi:10.1088/0959-5309/43/5/301

45. Wei W, Dong C, Morabito M, et al. Coarse-Grain Modeling of Shear-Induced Binding between von Willebrand Factor and Collagen. *Biophys J*. 2018;114(8):1816-1829. doi:10.1016/j.bpj.2018.02.017

46. Graessley WW, Hayward RC, Grest GS. Excluded-Volume Effects in Polymer Solutions. 2. Comparison of Experimental Results with Numerical Simulation Data. Published online 1999:3510-3517.

47. Flory PJ. *Principles of Polymer Chemistry*. Cornell University Press; 1953.

48. De Gennes PG. Coil-stretch transition of dilute flexible polymers under ultrahigh velocity gradients. *J Chem Phys*. 1974;5030(August 2003):5030-5042. doi:10.1063/1.1681018

49. Fowler WE, Erickson HP, Mckee PA, et al. Substructure of human von Willebrand factor . Substructure of Human von Willebrand Factor. 1985;76(4):1491-1500.

50. Dong X, Leksa NC, Chhabra ES, et al. The von Willebrand factor D'D3 assembly and structural principles for factor VIII binding and concatemer biogenesis. *Blood*. 2019;133(14):1523-1533. doi:10.1182/blood-2018-10-876300

51. Schwarzl R, Netz RR. Hydrodynamic shear effects on grafted and non-grafted collapsed polymers. *Polymers (Basel)*. 2018;10(8):27-30. doi:10.3390/polym10080926

52. Singh I, Themistou E, Porcar L, Neelamegham S. Fluid shear induces conformation change in human blood protein von Willebrand factor in solution. *Biophys J*. 2009;96(6):2313-2320. doi:10.1016/j.bpj.2008.12.3900

53. Shankaran H, Neelamegham S. Hydrodynamic Forces Applied on Intercellular Bonds, Soluble Molecules, and Cell-Surface Receptors. *Biophys J*. 2004;86(1 I):576-588. doi:10.1016/S0006-3495(04)74136-3

54. Tsai H, Sussman I, Nagel R. Shear stress enhances the proteolysis of von Willebrand factor in normal plasma. *Blood*. 1994;83(8):2171-2179. doi:10.1182/blood.v83.8.2171.2171

55. Bortot M, Sharifi A, Ashworth K, et al. Pathologic Shear and Elongation Rates Do Not Cause Cleavage of Von Willebrand Factor by ADAMTS13 in a Purified System. *Cell Mol Bioeng*. 2020;13(4):379-390. doi:10.1007/s12195-020-00631-2

56. Bortot M, Ashworth K, Sharifi A, et al. Turbulent Flow Promotes Cleavage of VWF (von Willebrand Factor) by ADAMTS13 (A Disintegrin and Metalloproteinase With a Thrombospondin Type-1 Motif, Member 13). *Arterioscler Thromb Vasc Biol*. 2019;39(9):1831-1842. doi:10.1161/ATVBAHA.119.312814

57. Soejima K, Nakamura H, Hirashima M, Morikawa W, Nozaki C, Nakagaki T. Analysis on the molecular species and concentration of circulating ADAMTS13 in blood. *J Biochem*. 2006;139(1):147-154. doi:10.1093/jb/mvj013

58. Zhang XF, Halverson K, Zhang C-Z, Wong WP, Springer TA. Mechanoenzymatic Cleavage of the Ultralarge Vascular Protein von Willebrand Factor. 2009;(June).

59. Batle J, Lopez-Fernandez MF, Lopez-Borrasca A, et al. Proteolytic Degradation Administration. *Blood*. 1987;70(1):173-176.

60. Cao W, Krishnaswamy S, Camire RM, Lenting PJ, Zheng XL. Factor VIII accelerates proteolytic cleavage of von Willebrand factor by ADAMTS13. Published online 2008. doi:10.1073/pnas.0801735105

61. Machha V, Tischer A, Moon-Tasson L, Auton M. The von Willebrand Factor A1-Collagen III

Interaction is Independent of Conformation and Type 2 von Willebrand Disease Phenotype. 2017;429(1):32-47. doi:10.1016/j.jmb.2016.11.014.The

62. Talpsep AKT. The von Willebrand factor collagen-binding activity assay : clinical application. Published online 2001:466-471. doi:10.1007/s002770100329

63. Nesbitt WS, Westein E, Tovar-Lopez FJ, et al. A shear gradient-dependent platelet aggregation mechanism drives thrombus formation. *Nat Med*. 2009;15(6):665-673. doi:10.1038/nm.1955

64. Humphrey W, Dalke A, Schulten K. {VMD} -- {V}isual {M}olecular {D}ynamics. *J Mol Graph*. 1996;14:33-38.

65. York D, Evensen NM, Martínez ML, De Basabe Delgado J. Unified equations for the slope, intercept, and standard errors of the best straight line. *Am J Phys*. 2004;72(3):367-375. doi:10.1119/1.1632486

66. Hill PD. Kernel Estimation of a Distribution Function. *Commun Stat - Theory Methods*. 1985;14(3):605-620. doi:10.1080/03610928508828937

67. Silverman BW. *Density Estimation for Statistics and Data Analysis*.; 1986. doi:10.3311/PPme.8017

Figure Captions

Figure 1. Free vs surface tethered VWF extension under flow. **A** Diagram illustrating[64] free-in-flow VWF (blue) vs surface-tethered (red) with applied shear flow. **B** Data from Schneider et al.[21] (blue) showing normalized extension vs shear stress for free VWF and data from Fu et al.[6] (red) showing normalized extension vs shear for tethered VWF. Required shear stress for free VWF extension is expected to be higher than required shear stress for surface tethered extension but experimentally the opposite was observed. **C** Predictions of mean extension in response to shear stress based on a Brownian dynamics model with a strong Lennard-Jones interaction potential proposed by Schneider et al.[21] for both a free-in-flow (blue) and tethered (red) polymer. Lengths are normalized based on the maximum observed length in the direction of flow.

Figure 2. Pulsed Laser Stroboscopic Imaging of Single molecules (PULSIS). **A** Basic schematic of the pressure driven flow system and imaging set up, not to scale. **B** Cartoon depiction of PULSIS. Objects are imaged with different duration pulses and by comparing the relative lengths, we can accurately measure the lengths of moving objects, and distinguish point objects from elongated objects. **C** Example experimental PULSIS trajectories of fluorescently labeled linearized DNA at 50 dyn/cm^2. **D** Example relationship between measured length of pulse L_m (μm) vs relative pulse duration T_p (arbitrary time units) for the two DNA PULSIS trajectories in 2C. For each trajectory, streak lengths are measured and a linear regression performed of the form $L_m=L_0+V*T_p$ with fitting errors according to York et al[65]. L_m is the illuminated streak length that we measure and T_p is the relative pulse duration defined by the pulse pattern (1, 2, or 3). The linear fit gives us the particle velocity V, and the y-intercept L_0 represents the length of the molecule observed with an infinitesimally short pulse i.e with no motion blur. The first trajectory (yellow) has a corrected length of 0.29 μm and resembles a compact object. The second trajectory has a corrected length of 1.03 μm and represents an elongated object. Error bars on pulse length are based on goodness of fit to predicted pulse shape (Supplemental Methods). **E** Positive control showing histogram of PULSIS determined lengths of double stranded M13 DNA plasmid both in supercoiled (blue) and linearized (red) state at 50 dyn/cm^2 imaged in sucrose buffer. Histograms are of motion blur-corrected lengths of hundreds of single molecules. The examples (trajectories and analysis) from figure 2C-D are two statistics from the linearized (red) distribution. Histograms are displayed along with kernel density estimates. Kernel density estimation is a method for smoothing histograms by applying a gaussian kernel to each point[66]. A Gaussian kernel was used with bandwidth set by Silverman's rule[67] **F** Negative control showing kernel density estimate for PULSIS motion blur corrected beads at different shear stress (manufacture determined diameter of 0.11 μm). Raw histograms in figure S1. Number of measurements, mean length and standard deviation for each condition are shown in panels E and F.

Figure 3. Free-in-flow VWF extension in shear flow. **A** Histogram of VWF length at 6 shear stresses (20, 50, 80, 100, 150, 200 dyn/cm^2). **B** Mean extension vs shear stress (o) and standard deviation vs shear stress (Δ) of VWF molecules for histograms shown in 3A. Monotonic increases in mean and standard deviation are both consistent with molecules extending under flow. **C** Percentiles 50-90 of VWF length vs shear stress for histograms in 3A. **D** Nonparametric statistical significance testing using Mann-Whitney U test comparing each shear stress length distribution. Values for $p<0.05$ indicate statistical significance. **E** Three example trajectories of VWF at 150 dyn/cm^2 with different PULSIS corrected lengths. Example molecules of a long, middle, and short extended molecule. **F** Corresponding plots of

pulse length vs relative pulse duration for trajectories in fig 3E. The y-intercept represents motion blur corrected lengths for VWF molecules.

Figure 4. Comparison of Brownian dynamics models for VWF. **A** Parameter space of the simulation as a function of bead diameter and Lennard-Jones interaction strength. Comparison with the size of spheres representing monomers of the different models. Sizes of spheres are on the same scale as 4B. Blue space represents collapsed polymers, with yellow being uncollapsed polymers. Dotted line represents the Θ-point where attractive and repulsive forces cancel out. **B** Electron microscopy images adapted from Fowler et al.[49] of VWF. **C** Comparison between Brownian dynamics simulation and experimental steady state extension for surface tethered polymers under shear flow. The three models are the original Lennard-Jones model (◇), the revised Lennard-Jones model (Δ) and the uncollapsed polymer model (□). Simulations compared to experimental data from previous surface stretching experiments of 2-3.5 µm VWF molecules from Fu et al. (o, 156 molecules measured)[6]. For each model and shear stress, the equilibrium extension of five independent simulations were averaged together at each shear stress. Extension is normalized by maximum extension and plotted on a semi log plot. Shaded area shows standard deviation of the 5 simulations. **D** Comparison of Brownian dynamics simulation and experimental mean extension for free-in-flow VWF with applied shear flow as measured by PULSIS, plotted on a semi log plot. Since the contour length of the experimental data is unknown, simulations and data are not normalized. Polymer simulation extensions were averaged over a time window and independent runs. (LJ original runs=3, Revised LJ runs = 3, Uncollapsed polymer runs = 10). Absolute contour length of all simulations was ~3 µm.

Figure 1.

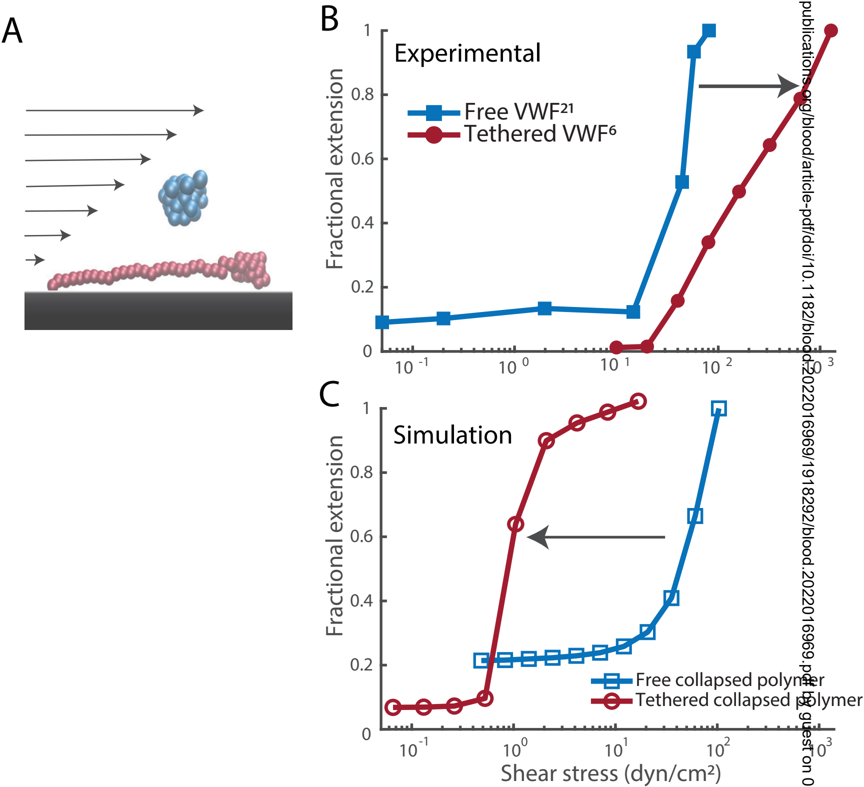
A
B
Experimental
Free VWF[21]
Tethered VWF[6]
Fractional extension
0
0.2
0.4
0.6
0.8
1
10 -1
10 0
10 1
10 2
10 3
C
Simulation
Free collapsed polymer
Tethered collapsed polymer
Fractional extension
0
0.2
0.4
0.6
0.8
1
10^{-1}
10^{0}
10^{1}
10^{2}
10^{3}
Shear stress (dyn/cm²)

Figure 2.

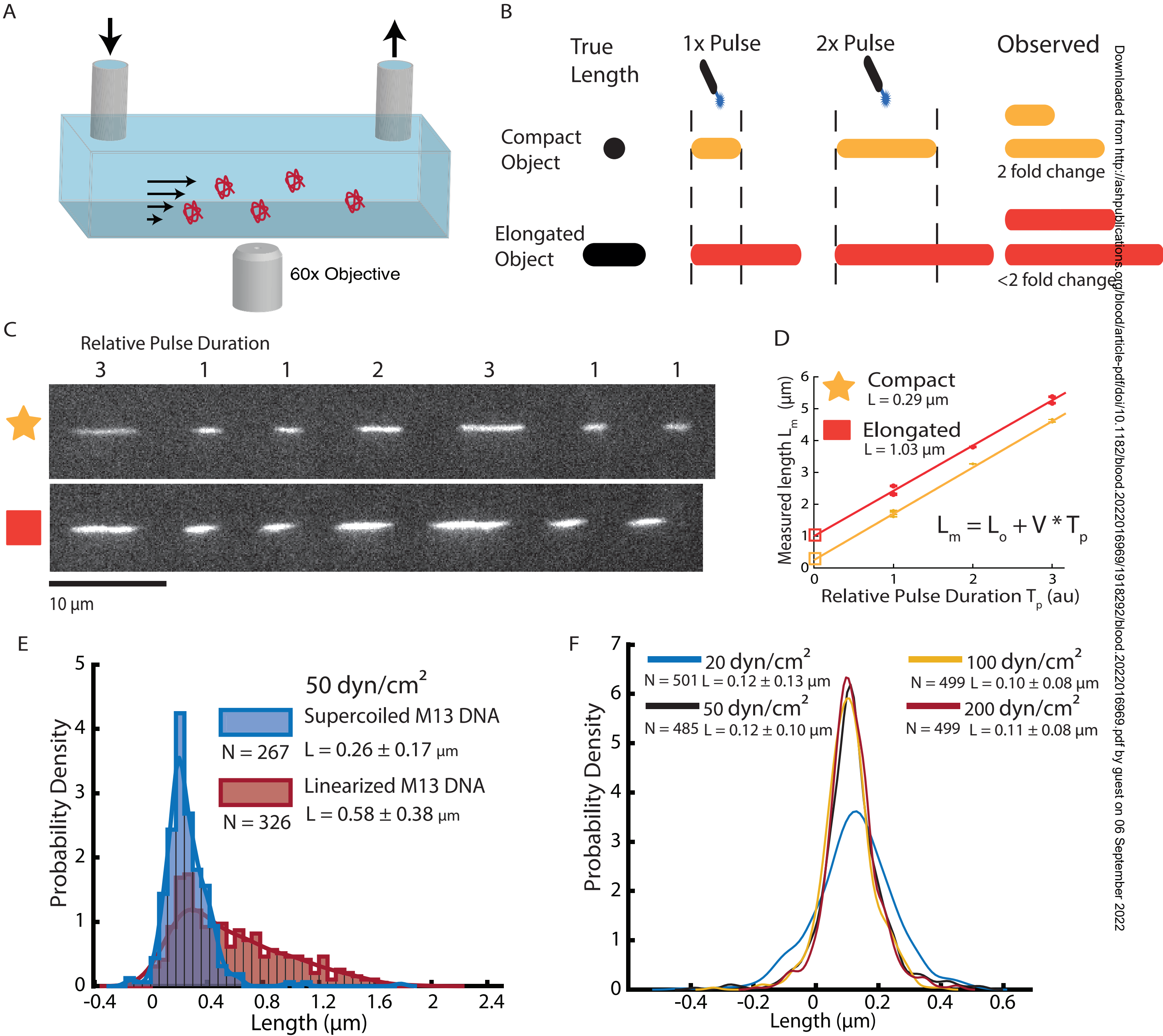
A
60x Objective
B
True Length
1x Pulse
2x Pulse
Observed
Compact Object
Elongated Object
2 fold change
<2 fold change
C
Relative Pulse Duration
3 1 1 2 3 1 1
10 µm
D
Compact
L = 0.29 µm
Elongated
L = 1.03 µm
Measured length L_m (µm)
L_m = L_o + V * T_p
Relative Pulse Duration T_p (au)
E
50 dyn/cm²
Supercoiled M13 DNA
N = 267 L = 0.26 ± 0.17 µm
Linearized M13 DNA
N = 326 L = 0.58 ± 0.38 µm
Probability Density
Length (µm)
F
20 dyn/cm²
N = 501 L = 0.12 ± 0.13 µm
50 dyn/cm²
N = 485 L = 0.12 ± 0.10 µm
100 dyn/cm²
N = 499 L = 0.10 ± 0.08 µm
200 dyn/cm²
N = 499 L = 0.11 ± 0.08 µm
Probability Density
Length (µm)

Figure 3.

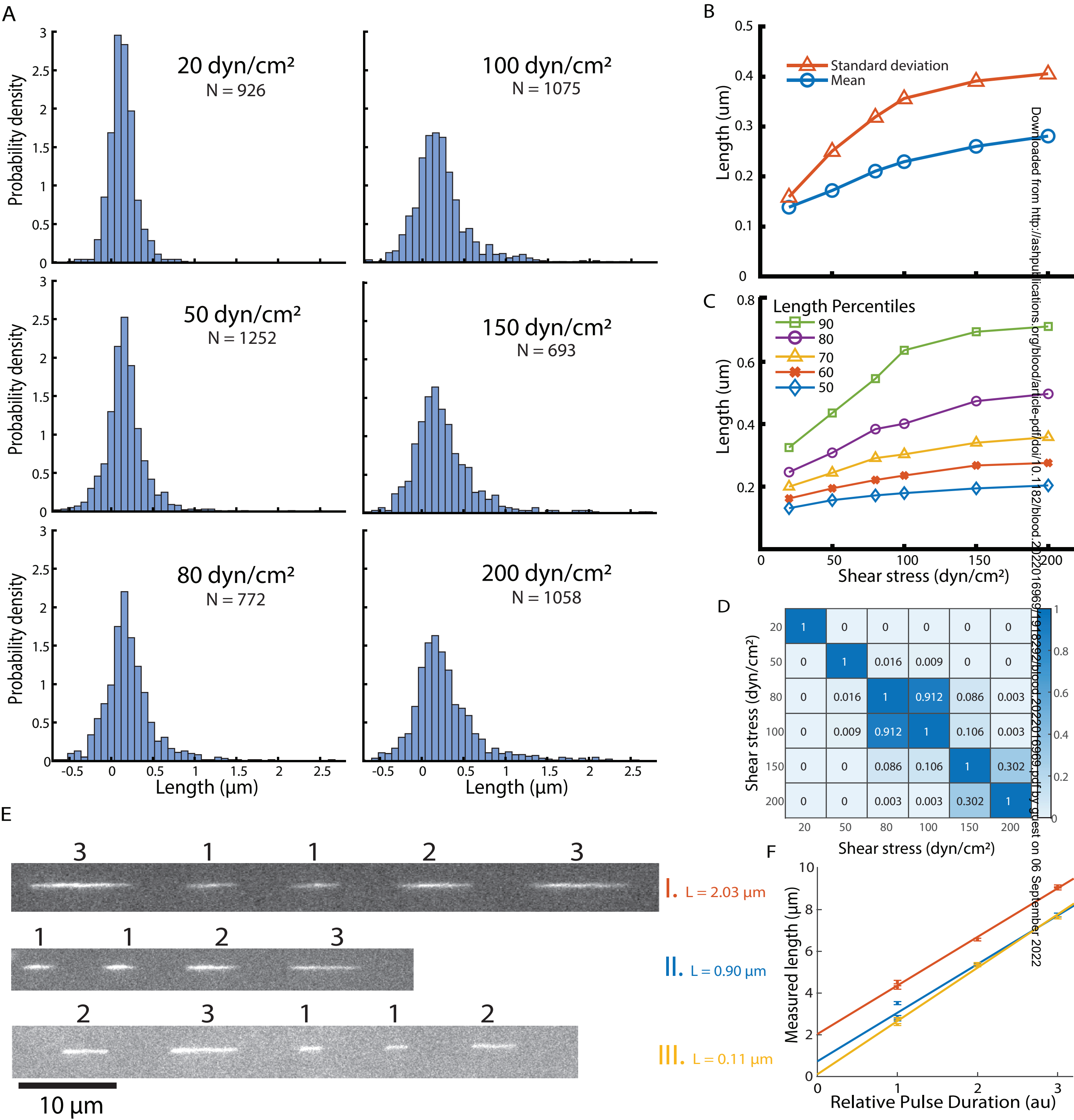
A
20 dyn/cm²
N = 926
100 dyn/cm²
N = 1075
50 dyn/cm²
N = 1252
150 dyn/cm²
N = 693
80 dyn/cm²
N = 772
200 dyn/cm²
N = 1058
Probability density
Length (μm)
B
Standard deviation
Mean
Length (um)
C
Length Percentiles
90
80
70
60
50
Length (um)
Shear stress (dyn/cm²)
D
Shear stress (dyn/cm²)
E
I. L = 2.03 μm
II. L = 0.90 μm
III. L = 0.11 μm
10 μm
F
Measured length (μm)
Relative Pulse Duration (au)

Figure 4.

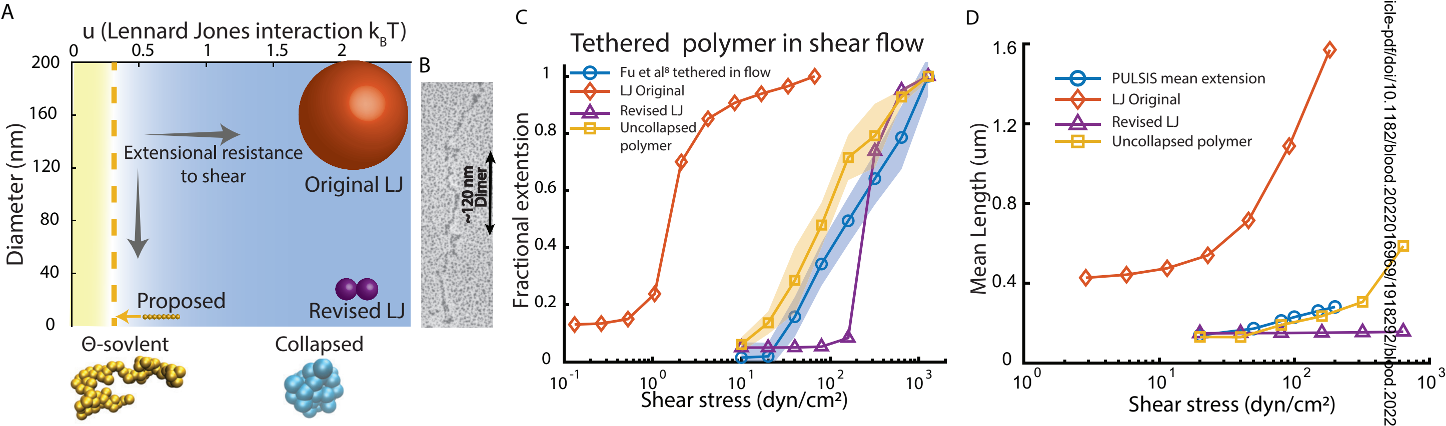
A
u (Lennard Jones interaction k_BT)
0
0.5
1
1.5
2
Diameter (nm)
200
160
120
80
40
0
Extensional resistance
to shear
Original LJ
Proposed
Revised LJ
Θ-sovlent
Collapsed
B
~120 nm
Dimer
C
Tethered polymer in shear flow
Fu et al[8] tethered in flow
LJ Original
Revised LJ
Uncollapsed
polymer
Fractional extentsion
Shear stress (dyn/cm²)
D
PULSIS mean extension
LJ Original
Revised LJ
Uncollapsed polymer
Mean Length (um)
Shear stress (dyn/cm²)